



HAL
open science

An Automatic Riemannian Artifact Rejection Method for P300-based BCIs

Davoud Hajhassani, Jérémie Mattout, Marco Congedo

► **To cite this version:**

Davoud Hajhassani, Jérémie Mattout, Marco Congedo. An Automatic Riemannian Artifact Rejection Method for P300-based BCIs. European signal processing conference 2024, Aug 2024, Lyon, France. hal-04645211

HAL Id: hal-04645211

<https://hal.science/hal-04645211>

Submitted on 11 Jul 2024

HAL is a multi-disciplinary open access archive for the deposit and dissemination of scientific research documents, whether they are published or not. The documents may come from teaching and research institutions in France or abroad, or from public or private research centers.

L'archive ouverte pluridisciplinaire **HAL**, est destinée au dépôt et à la diffusion de documents scientifiques de niveau recherche, publiés ou non, émanant des établissements d'enseignement et de recherche français ou étrangers, des laboratoires publics ou privés.

An Automatic Riemannian Artifact Rejection Method for P300-based BCIs

Davoud Hajhassani

Team ViBS, GIPSA-lab

University Grenoble Alpes, CNRS
Grenoble, France

0009-0008-6674-5546

J eremie Mattout

Brain Dynamics and Cognition Team

Lyon Neuroscience Research Center, INSERM
Lyon, France

0000-0003-2659-6984

Marco Congedo

Team ViBS, GIPSA-lab

University Grenoble Alpes, CNRS
Grenoble, France

0000-0003-2196-0409

Abstract—This paper presents a completely automatic artifact rejection method for electroencephalographic data based on Riemannian geometry. The proposed method is tested on two P300-based brain-computer interface databases and is shown to allow superior accuracy and information transfer rate as compared to two state-of-the-art methods.

Index Terms—Riemannian geometry, Electroencephalography (EEG), Brain-computer interface (BCI), Artifacts, P300 classification

I. INTRODUCTION

Brain-computer interface (BCI) systems facilitate communication between the brain and computers by the online interpretation of brain signals. Brain signals can be recorded through different invasive and non-invasive neuroimaging techniques [1], among which the most widely spread and consolidated is electroencephalography (EEG). EEG provides a non-invasive, minimally restrictive, relatively low-cost measure of mesoscopic brain dynamics with high temporal resolution and portability for clinical use [2]. Over the last three decades, EEG-based BCI systems have emerged as a promising approach across various proof-of-concept applications. These include controlling wheelchairs and prosthetics, navigating cursors on screens, spellers, gaming, and artistic expression [3], [4], [5].

Despite all the benefits and applications, EEG is susceptible to contamination by various types of artifacts, i.e., electrical signals that do not originate in the brain. They are endogenous (e.g. biological sources such as ocular, muscle, and cardiac activity) or exogenous (e.g. instrumental and environmental sources such as impedance mismatch, electromagnetic interference, etc.) and often exhibit significant amplitudes that severely degrade the signal-to-noise ratio, rendering many applications impractical. EEG signals are inherently weak, typically a few to a few tens of μV , requiring amplification, which also amplifies artifacts [6]. Due also to the non-linear characteristics of these artifacts, isolating them without losing genuine neuronal data has proved to be a formidable task. Nonetheless, in real-time EEG-based BCIs, where system performance depends on current data quality, the existence of artifacts has the potential to disrupt the feedback stream.

This work has been supported by ANR grant HiFi project (ANT-20-CE17-0023).

These hurdles underscore the significance of incorporating an artifact-handling stage in the EEG signal analysis pipeline that would effectively eliminate artifacts [7].

In the literature, numerous artifact removal techniques have been introduced [8]. They fall into two main categories: *artifact correction* techniques, which aim at modifying or adjusting the recorded signal to mitigate artifacts while preserving as much as possible the genuine EEG data, and *artifact rejection* techniques, which aim at identifying and discarding segments of data containing artifacts. It is worth mentioning that some methods are hybrid.

The general strategy of existing methods is to assess several data metrics and correct or reject data epochs exceeding threshold values. Due to the large variability of EEG data and, even more, artifacts, the common problem they face is that fixed thresholds are sub-optimal and often times clearly inappropriate. Instead, the thresholds should be data-specific and should automatically *adapt* to the data. This study focuses on such a strategy for artifact rejection.

Widely used software tools like Brainstorm [9], EEGLAB [10], and MNE [11] offer the capability to identify and exclude data segments affected by artifacts. Pipeline-based approaches like Fully Automated Statistical Thresholding for EEG Artifact Rejection (FASTER) employ fixed thresholds derived from classical Gaussian statistics to detect artifacted data segments and sensors [12]. Also, methods like PREP are tailored to detect and correct artifacted sensors but do not offer a solution for eliminating artifacted data segments [13]. A popular method is AutoReject (AR), an automatic algorithm for the rejection and correction of artifacted data segments. This method employs cross-validation and a robust evaluation metric to estimate the optimal threshold. Furthermore, it is expanded into an algorithm capable of estimating this threshold for each sensor [14].

A somehow different approach is offered by the Riemannian Potato (RP) [15], a multivariate artifact rejection method using Riemannian geometry [16]. The feature of interest is simply the covariance matrix of EEG epochs. The RP estimates the barycenter of all epochs and assesses the distance of the epochs from the barycenter using appropriately derived z-scores. It has been intensively used for online artifact rejection for P300-based BCI spellers [17] and games [18], offline rejection

before the statistical analysis of cognitive assessments [19], and epilepsy detection [20]. A major drawback of RP is reduced sensitivity and specificity as the number of sensors increases.

Various improvements have been suggested for RP, such as incorporating robust mean estimation through outlier removal [21] and employing geometric z-scores in place of arithmetic z-scores [22]. The Riemannian Potato Field (RPF) [24] represents the latest advancement, encompassing a generalization and extension of RP. The RPF overcomes the degradation induced by an increase in the number of sensors by using several potatoes of low dimension in parallel, each one designed to capture a particular class of artifacts that affects specific spatial areas at specific frequency bands. Eventually, the output z-scores of all potatoes (i.e., a potato field) are combined into a single p-value using the right-tail Fisher's combination function [23], allowing a Signal Quality Index (SQI) for each epoch ranging from 1 (clean) to 0 (noisy) [24].

As many other artefact rejection methods, the RP and RPF also use fixed thresholds. In this work, we present an improved Riemannian Potato Field artifact rejection method (iRPF) that adaptively sets all required thresholds. Besides being fully automatic, the iRPF improves upon the RPF in several other ways, as we will present.

We evaluate the effectiveness of the presented iRPF method by comparing the accuracy and information transfer rate (ITR) obtained by the iRPF, RPF and AR on two publicly available P300-based BCI experiments.

II. METHODS AND MATERIALS

In this section we denote matrices by upper case bold letters (\mathbf{A}), variables by lower case italic letters (a), and constants by upper case italic letters (A). The matrix operators $(\cdot)^T$, $(\cdot)^{-1/2}$, $\text{Log}()$ and $\|\cdot\|_F$ denote the transpose, inverse of the principal square root, logarithm, and Frobenius norm of the argument, respectively.

A. Geometry of Covariance Matrices

In the context of EEG signal analysis, $\mathbf{X} \in \mathbb{R}^{N \times T}$ represents an epoch, recorded across N channels/electrodes and T temporal samples. If the signal is centered, such as after applying band-pass filtering, the maximum-likelihood estimator of the covariance matrix is $\mathbf{\Sigma} = \frac{1}{N-1} \mathbf{X} \mathbf{X}^T \in \mathbb{R}^{N \times N}$. The efficiency of this estimator requires T to significantly exceed N . For other estimators the interested reader is directed to [25]. The affine-invariant Riemannian distance between two points $\mathbf{\Sigma}_1$ and $\mathbf{\Sigma}_2$ is given by

$$\delta_R(\mathbf{\Sigma}_1, \mathbf{\Sigma}_2) = \|\text{Log}(\mathbf{\Sigma}_1^{-\frac{1}{2}} \mathbf{\Sigma}_2 \mathbf{\Sigma}_1^{-\frac{1}{2}})\|_F = \left(\sum_{n=1}^N \frac{1}{2} \log^2 \lambda_n \right)^{\frac{1}{2}},$$

where λ_n , $n = 1, \dots, N$, are the eigenvalues of $\mathbf{\Sigma}_1^{-\frac{1}{2}} \mathbf{\Sigma}_2 \mathbf{\Sigma}_1^{-\frac{1}{2}}$. The barycenter, or geometric mean, of I matrices $\mathbf{\Sigma}_i$, where $i = 1, \dots, I$, is defined as the matrix that minimizes the dispersion such as

$$\bar{\mathbf{\Sigma}} = \arg \min_{\mathbf{\Sigma} \in \mathcal{M}_C} \sum_{i=1}^I \delta_R^2(\mathbf{\Sigma}_i, \mathbf{\Sigma}).$$

The baycenter can be estimated by iterative algorithms such as the gradient descent algorithms or the more efficient fixed-point algorithm outlined in [26].

B. Riemannian Potato

The merit of the Riemannian Potato (RP) method [15] has been to introduce multivariate features for detecting artifacts. The idea is to represent EEG epochs as covariance matrices, estimate a barycenter $\bar{\mathbf{\Sigma}}$ of them and obtain a z-score quantifying the distance of each epoch from the barycenter. The goal is to identify and remove epochs whose covariance matrix significantly deviates from the expected value. The method is both sensitive and specific as long as the barycenter represents clean EEG data. The implementation is simple: for each epoch indexed by i , the Riemannian distance between the i th covariance matrix $\mathbf{\Sigma}_i$ and the reference $\bar{\mathbf{\Sigma}}$ is computed as $d_i = \delta_R(\mathbf{\Sigma}_i, \bar{\mathbf{\Sigma}})$. Then, the z-score z_i of this distance is computed as $z_i = \frac{d_i - \mu}{\sigma}$, where μ and σ are the mean and the standard deviation of the distances to the reference matrix. The z-score is employed to represent the dispersion of covariance matrices deemed as clean, establishing a SQI and allowing the estimation of a suitable threshold z_{th} to delineate the rejection region.

C. Riemannian Potato Field

The RP method has been expanded and improved in [24]. Due to the multivariate nature of the potato, artifacts that cause a significant variation in one or a few channels only may not determine a large deviation of the whole covariance matrix from the barycenter, thus such artifacts may remain undetected. This phenomenon can occur for a headset with as few as $N = 8$ sensors. To address this limitation, the RPF introduces and integrates several potatoes of smaller dimensions. Each of these potatoes is defined to capture specific artifacts that typically affect particular spatial regions (e.g., subsets of channels) in specific frequency bands. The z-scores resulting from all potatoes are then combined into a unified p-value, which serves as a SQI. Depending on the available channels, various potatoes are defined to identify different types of potential artifacts. For instance, in order to address ocular artifacts, a potato is defined using EOG and/or forehead electrodes with signal low-pass filtered below 7 Hz. When it comes to muscular artifacts, multiple potatoes can be defined using external electrodes and an high-pass filter above 20Hz. These may include a potato defined using temporal electrodes to identify jaw clenching and swallowing.

After defining a set of J potatoes comprising the RPF, their output z-scores are combined into a single p-value using the Fisher's combination method [23]. For z-scores z_j , $j = 1, \dots, J$, their corresponding p-values p_j are obtained by $p_j = 1 - \text{cdf}_{N_{0,1}}(z_j)$, where cdf_D represents the cumulative distribution function of D , and $N_{0,1}$ represents the normal distribution with mean 0 and standard deviation 1.0. The Fisher's function combines the p-values p_j as $q = -2 \sum_{j=1}^J \log(p_j)$.

Under the assumption of normality of the z-scores q is distributed as a chi-square with $2J$ degrees of freedom, thus its p-

value $p = 1 - \text{cdf}_{\chi^2_{2J}}(q)$ is uniformly distributed. However, the z-scores of Riemannian distances are not normally distributed, thus p is not uniformly distributed in general. This implies that the threshold is not meaningful in absolute terms. More importantly, while one may still be able to empirically set an effective threshold, the optimal value strongly depends on the data, to which the threshold should adapt. This is a major limitation of the RP and RPF and will be addressed in the next section.

The RPF method also introduces a robust barycenter estimators. In fact, while the Riemannian barycenter offers much greater robustness as compared to the Euclidean mean [16], it can nonetheless be affected by outliers if they are numerous and/or very deviant. The robust estimator iterates the barycenter estimation a fixed number of steps (typically, three to five) excluding at each step all covariance matrices featuring a z-score superior to a pre-defined threshold [21], [25]. The iRPF we present in the next section gets rid of this hyperparameter as well.

D. Improved Riemannian Potato Field

The present method, iRPF, improves upon the RPF in several ways:

- the robust barycenter estimations are obtained with an adaptive algorithm that does not require fixing a threshold. At each step, the z-scores of the distance from the current barycenter estimations are sorted in ascending order and an in-house knee-detection method is used to determine the number of points to be discarded in subsequent steps. The procedure stops as soon as no knee is detected or when four steps have been carried out.

- The RP and RPF rely exclusively on the Riemannian distance of covariance matrices to the barycenter. We introduce here two more features: the trace and the Frobenius norm of the covariance matrices. The trace feature is particularly useful to detect artifacts that do not co-vary across sensors. For instance, EMG artifacts can be better detected using as feature the trace of the covariance matrix comprising external contralateral sensors such as (T4, T5), (T7, T8), etc. The Frobenius norm, on the opposite, is particularly useful to detect artifacts that are expected to co-vary across sensors (regardless the sign of the co-variation). For instance, lateral eye movements are better detected using as feature the Frobenius norm of the covariance matrix comprising contralateral frontal electrodes such as (F7-F8) and/or (F3-F4). As for the distance metric, the z-scores of the trace and Frobenius norm features are computed, converted in p-values and combined.

- The RPF employs the Fisher combination function of the p-values obtained for each potato. In the present contribution we introduce the use of other p-value combination functions, namely, the Liptak and Tippett functions [28] and their meta-combination, that is, the combination of several combination functions. This allows greater flexibility leveraging the strength of several combination functions.

- The last improvement of the iRPF method is the automatic and adaptive determination of the p-value threshold used

to reject artifacted epochs. While in the RPF method this threshold is pre-defined, we apply a published knee-detection algorithm [29], which adapts to the data.

E. Description of P300 Speller

In ERP-based BCIs a continuous sequence of discrete sensory stimuli consisting in flashing symbols, is sequentially presented on a screen. Users can choose symbols one at a time by directing their attention to them. In the case of P300 spellers, these symbols constitute a subset of those typically found on a computer keyboard. The symbol the user wish to select is referred to as "Target", whereas all other symbols are referred to as "Non-target". Upon flashing, all symbols evoke stereotypical electrical potentials in the brain, lasting up to one second, which are different for target and non-target symbols. This enables the possibility to operate classification. Detecting a target at a single-trial level is challenging, prompting character classification after multiple repetitions to accumulate evidence and enhance accuracy. Once several repetitions are completed, the classifier predicts the character, preparing to initiate another round of character prediction [30].

F. Description of Data

This study analyzes two P300-based BCI databases [31], [32], which are publicly available on MOABB framework [33]. The principal characteristics of which are outlined in Table I.

TABLE I
PRINCIPAL CHARACTERISTICS OF DATABASES USED IN THIS STUDY

Dataset	Subjects	Channels	Characters per subject	Trielas (Target/Non-target)
BNCI2014008	8	8	35	20/100
BNCI2014009	10	16	18	16/80

G. Pipeline

The raw EEG signals are band-pass filtered in the 1-24 Hz region using a forward-backward Butterworth IIR filter and down-sampled to 128 Hz using a natural cubic spline routine. Following this minimal pre-processing step, trials of one second are extracted starting at the onset of the flashes. Preprocessing was performed using the MNE Python package [11]. In order to evaluate the effect of artifact rejection we employ a character-level classification scheme named Bayesian Accumulation of Riemannian Probabilities (ASAP) [34]. As classifier, we use the Riemannian Minimum Distance to mean [35]. For each subject and session, the training set consists of trials associated with the initial six or twelve characters, while the test set comprises the remaining trials. The ongoing experiment involves within-session classification of P300-speller characters, aiming to compare both accuracy and information transfer rate (ITR) without using artifact rejection or using Autoreject (AR), the Riemannian Potato Field (RPF) with three rejection thresholds (0.5, 0.1, 0.05) and the presented improved Riemannian Potato Field (iRPF). The potato fields we have employed are detailed in Table II. They have been using also for the RPF method applying for all potatoes the

covariance distance metric. As p-value combination for the iRPF, we have used the Tippett meta-combination of the Fisher and Liptak combination. For ASAP, AR and RPF we have used the Python packages ASAP [37], autoreject [14] and pyRiemann [36], respectively. We have implemented the IRPF method in the Julia programming language and then exported it onto the Python environment.

TABLE II
DEFINED POTATO FIELD

Dataset	Potatoes	Metric	Frequency range (Hz)
BNCI2014008	P3 P4	trace	16-24
	PO7 PO8	trace	16-24
	Oz Pz	trace	16-24
	all available channels	cov	1-24
BNCI2014009	F3 Fz F4	norm	1-7
	F3 Fz F4	trace	16-24
	PO7 Oz PO8	trace	16-24
	FCz C3 Cz C4		
	CP3 CPz CP4 P3 Pz	cov	1-24
	P4 PO7 PO8 Oz		

III. RESULTS

Fig. 1 and Fig. 2 illustrate the accuracy of character classification, defined as the proportion of characters correctly classified and the ITR in bits per minute as a function of the number of repetitions, averaged across all subjects and sessions. While the accuracy increases monotonically as the number of repetitions increases, the optimal ITR is achieved within two or three repetitions. Overall, the iRPF allows both better accuracy and higher ITR with three or more repetitions. For the RPF, there is not a specific rejection threshold performing better than the others. As expected, the variability of the optimal rejection threshold across sessions is very high (data not shown). The execution time of different artifact rejection methods is reported in Table III.

TABLE III
EXECUTION TIME IN SECONDS FOR DIFFERENT ARTIFACT REJECTION METHODS

Dataset	AR	RPF	iRPF
BNCI2014008	1235	247	92
BNCI2014009	713	185	131

IV. DISCUSSION

We have presented the improved Riemannian Potato Field (iRPF), a completely automated method for obtaining a signal quality index of EEG epochs and allowing the rejection of epochs contaminated by artifacts. In contrast to its predecessor (RPF [24]), the method adapts to the data in order to find automatically the relevant rejection threshold. In our opinion this is an important advance for an artifact rejection method that ought to be used on a large scale.

The iRPF is a very flexible method. Indeed, virtually any kind of EEG artifact can be detected defining the appropriate Riemannian potato(s). The other side of the coin is that the

definition of the potato field, i.e., the set of potatoes to be monitored, can greatly influence the SQI and the ensuing rejection region. An interesting research direction concerns the development of a tool to define an appropriate potato field given the data, the available EEG leads and the sought objective of the iRPF.

REFERENCES

- [1] L. Fernando Nicolas-Alonso, J. Gomez-Gil, "Brain Computer Interfaces, a Review," *Sensors* 12, no. 2, 2012.
- [2] R. Abiri, S. Borhani, E. Sellers, Y. Jiang, X. Zhao, "A comprehensive review of EEG-based brain-computer interface paradigms," *J. Neural Eng.* vol. 16, no. 1, 2019.
- [3] L. Korczowski, A. Barachant, A. Andreev, C. Jutten, M. Congedo, "Brain invaders 2: An open-source plug & play multi-user BCI videogame," in *Proc. 6th Int. Brain-Comput. Interface Meeting*, 2016.
- [4] D. J. McFarland, J. R. Wolpaw, "Brain-computer interfaces for communication and control," *Commun. Assoc. Comput. Machinery*, vol. 54, no. 5, pp. 60–66, 2011.
- [5] X. Gu, Z. Cao, A. Jolfaei, P. Xu, D. Wu, T.-P. Jung, C.-T. Lin, "EEG-based Brain-Computer Interfaces (BCIs): A Survey of Recent Studies on Signal Sensing Technologies and Computational Intelligence Approaches and Their Applications," in *IEEE/ACM Tran. on Comput. Bio. and Bio.*, 2021.
- [6] A. Bashashati, M. Fatourehchi, R.K Ward, G.E Birch, "A survey of signal processing algorithms in brain-computer interfaces based on electrical brain signals," *Journal of Neural Engineering*, 2007.
- [7] M.M.N. Mannan, M.A. Kamran, M.Y. Jeong, "Identification and removal of physiological artifacts from electroencephalogram signals: a review," *IEEE Access*, 2018.
- [8] D. Gorjan, K. Gramann, K. De Pauw, U. Marusic, "Removal of movement-induced EEG artifacts: current state of the art and guidelines," *J Neural Eng.*, 2022.
- [9] F. Tadel, S. Baillet, J.C. Moshier, D. Pantazis, R.M. Leahy, "Brainstorm: a user-friendly application for MEG/EEG analysis," *Comput. Intell. Neurosci.*, 2011.
- [10] A. Delorme, S. Makeig, "EEGLAB: an open source toolbox for analysis of single-trial EEG dynamics including independent component analysis," *J. Neurosci. Methods*, 2004.
- [11] A. Gramfort, M. Luessi, E. Larson, et al., "MNE software for processing MEG and EEG data," *NeuroImage*, V. 86, 2014.
- [12] H. Nolan, R. Whelan, R.B. Reilly, "FASTER: Fully Automated Statistical Thresholding for EEG artifact Rejection," *J. Neurosci. Methods*, 2010.
- [13] N. Bigdely-Shamlo, T. Mullen, Ch. Kothe, K.M. Su, A.K. Robbins, "The PREP pipeline: standardized preprocessing for large-scale EEG analysis," *Front. in Neur. info.*, v. 9, 2015.
- [14] M. Jas, D.A. Engemann, Y. Bekhti, F. Raimondo, A. Gramfort, "Autoreject: Automated artifact rejection for MEG and EEG data," *NeuroImage*, volume 159, 2017.
- [15] A. Barachant, A. Andreev, M. Congedo, "The Riemannian Potato: an automatic and adaptive artifact detection method for online experiments using Riemannian geometry," *TOBI Workshop IV*, Sion, Switzerland, 2013.
- [16] Marco Congedo, Alexandre Barachant, Rajendra Bhatia, "Riemannian geometry for EEG-based brain-computer interfaces; a primer and a review," *Brain-Computer Interfaces*, 2017.
- [17] L. Mayaud, S. Cabanilles, A. Van Langenhove, M. Congedo, et al., "Brain-computer interface for the communication of acute patients: a feasibility study and a randomized controlled trial comparing performance with healthy participants and a traditional assistive device," *Brain-Computer Interfaces*, vol. 3, pp. 197–215, 2016.
- [18] A. Andreev, A. Barachant, F. Lotte, M. Congedo, "Brain-Computer Interfaces 2: Technology and Applications," John Wiley; Sons, 2016, ch. 14 - Recreational Applications of OpenViBE: Brain Invaders and Use-the-Force, pp. 241–257.
- [19] G. Borghini, P. Arico, F. Ferri, I. Graziani, S. Pozzi, L. Napolitano, et al., "A neurophysiological training evaluation metric for air traffic management," in *Int Conf IEEE Eng. , EMBC*, 2014.
- [20] Y. Ru, J. Li, Z. Wei, "Epilepsy Detection Based on Riemann Potato in Noisy Environment," *Appl. Bionics. Biomech.*, 2022.

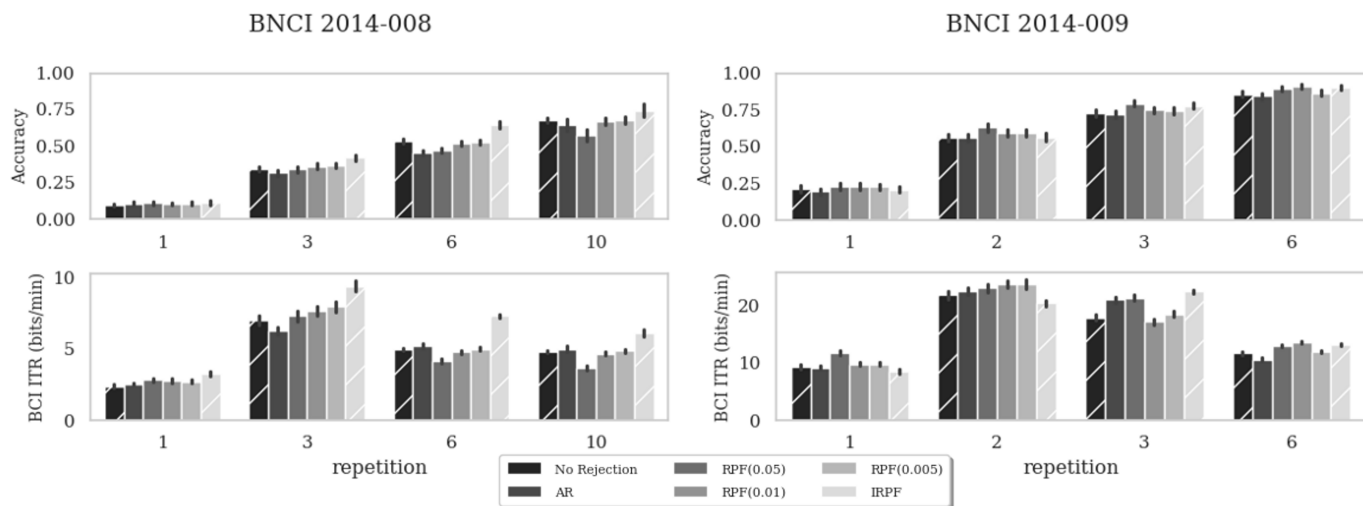


Fig. 1. Accuracy (proportion of correctly classified characters) (top) and information transfer rate (bottom) averaged across all characters and subjects for the BNCI2014-008 dataset (left) and the BNCI2014-009 dataset (right). The training set comprises the first six characters.

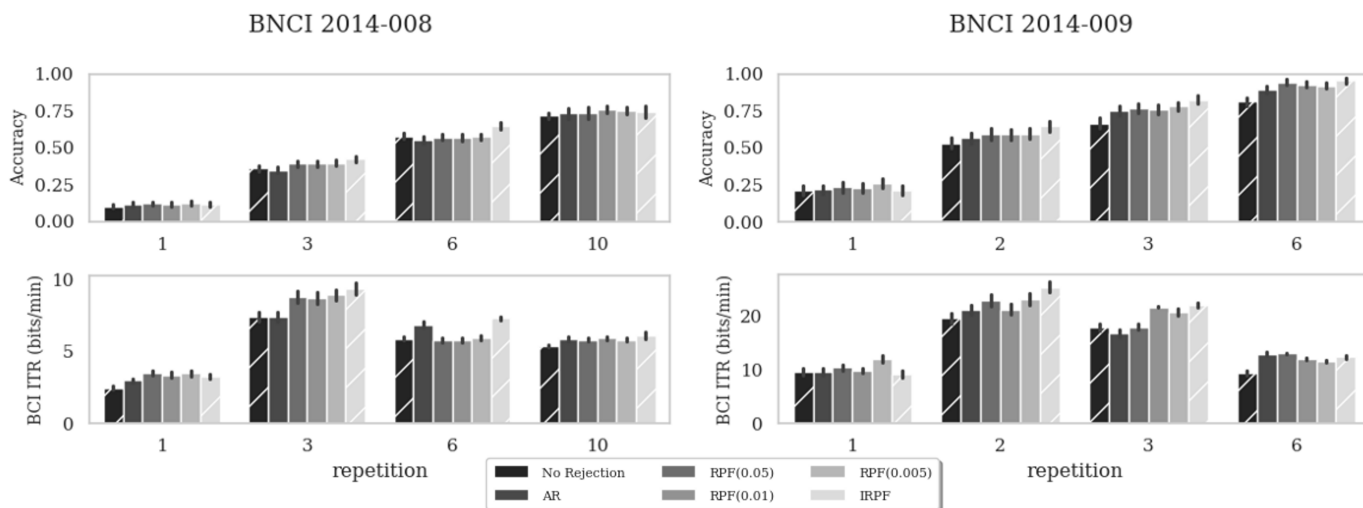


Fig. 2. As per Fig. 1 except the training set comprises the first twelve characters.

- [21] E. K. Kalunga, S. Chevallier, Q. Barthelemy, K. Djouani, Y. Hamam, E. Monacelli, "From Euclidean to Riemannian Means: Information Geometry for SSVEP Classification," in *Int Conf on GSI*, 2015.
- [22] M. Congedo, "EEG source analysis," Grenoble University, Tech. Rep. HDR, 2013.
- [23] R. Fisher, "Statistical Methods for Research Workers," Oliver and Boyd, 1925.
- [24] Q. Barthelemy, L. Mayaud, D. Ojeda, M. Congedo, "The Riemannian Potato Field: A Tool for Online Signal Quality Index of EEG," *IEEE Trans Neural Syst Rehabil Eng*, 2019.
- [25] E. K. Kalunga, S. Chevallier, Q. Barthelemy, K. Djouani, E. Monacelli, Y. Hamam, "Online SSVEP-based BCI using Riemannian geometry," *Neurocomputing*, vol. 191, pp. 55–68, 2016.
- [26] M. Congedo, A. Barachant, E. K. Koopaeei, "Fixed Point Algorithms for Estimating Power Means of Positive Definite Matrices," in *IEEE Trans. on Signal Processing*, vol. 65, no. 9, pp. 2211–2220, 2017.
- [27] M. Congedo, B. Afsari, A. Barachant, M. Moakher, "Approximate Joint Diagonalization and Geometric Mean of Symmetric Positive Definite Matrices," *PLoS one*, April 28, 2015.
- [28] N. A. Heard, P. Rubin-Delanchy, "Choosing between methods of combining p-values," *Biometrika*, v. 105, Issue 1, March 2018.
- [29] V. Satopaa, J. Albrecht, D. Irwin, B. Raghavan, "Finding a "Kneedle" in a Haystack: Detecting Knee Points in System Behavior," 2011 31st Int. Conf. on Dist. Comput. Sys. Workshops, Minneapolis, MN, USA, pp. 166–171, 2011.
- [30] M. Congedo, L. Korczowski, A. Delorme, F. Lopes Da Silva, "Spatio-Temporal Common Pattern; a Companion Method for ERP Analysis in the Time Domain," *J Neurosci Methods*, 267: 74–88, 2016.
- [31] A. Riccio, L. Simione, F. Schettini, et al., "Attention and P300-based BCI performance in people with amyotrophic lateral sclerosis," *Front Hum Neurosci.*, 2013.
- [32] F. Aloise, P. Aricò, F. Schettini, et al., "A covert attention P300-based brain-computer interface: Geospell," *Ergonomics*, 2012.
- [33] V. Jayaram, A. Barachant, "MOABB: trustworthy algorithm benchmarking for BCIs," *J Neural Eng.* 2018;15(6):066011.
- [34] Q. Barthelemy, S. Chevallier, R. Bertrand-Lalo and P. Clisson, "End-to-end P300 BCI using Bayesian accumulation of Riemannian probabilities," *Brain-Computer Interface*, vol. 10, pp. 50–61, 2022.
- [35] A. Barachant, S. Bonnet, M. Congedo, and Ch. Jutten, "Multiclass Brain-Computer Interface Classification by Riemannian Geometry," *IEEE Transactions on Biomedical Engineering*, 2012.
- [36] <https://pyriemann.readthedocs.io/>.
- [37] <https://github.com/sylvchev/asap-p300-bci>.